ACS OMEGA

Open Access

http://pubs.acs.org/journal/acsodf

Article

Negative Capacitance Dual-Gated ISFETs as Ultra-Sensitive pH Sensors

Fahimul Islam Sakib,[§] Md. Azizul Hasan,[§] Mumtahena Diyan Mohona, and Mainul Hossain*

Cite This: *ACS Omega* 2023, 8, 48756−48763

Read Online

ACCESS | Metrics & More | Article Recommendations

ABSTRACT: Ion-sensitive field-effect transistors (ISFETs) are promising candidates for next-generation pH sensors, enabling highly sensitive and label-free biomolecular and chemical detection. Emerging FETs based on the negative capacitance (NC) effect offer steep-subthreshold switching and higher drive current simply by integrating a ferroelectric (FE) material into the gate stack. Here, we propose a novel NC dual-gated ISFET (NC-DG-ISFET)-based pH sensor, with FE layers integrated into both the top and the bottom gate stacks. The current and voltage sensitivities of the proposed device are extracted from its transfer characteristics, obtained by combining the numerical solutions of the one-dimensional (1D) Landau-Khalatnikov (L-K) equation with three-dimensional (3D) technology computer-aided design (TCAD) simulations. Results show that the NC-DG-ISFET can surpass the sensitivity of some of the state-of-the-art DG-ISFET pH sensors. The inclusion of the FE layers into the gate stacks of a baseline DG-ISFET leads to 51% reduction in subthreshold swing (SS), causing a 5× increase in current sensitivity (S_I) in the subthreshold region of operation and a 2× increase in voltage sensitivity (S_V). The influence of channel thickness and channel length on the sensor performance is also invesitgated. The findings presented here provide a new pathway to leverage the steep-switching behavior of NCFETs for the next generation of highly sensitive and label-free DG-ISFET pH sensors.

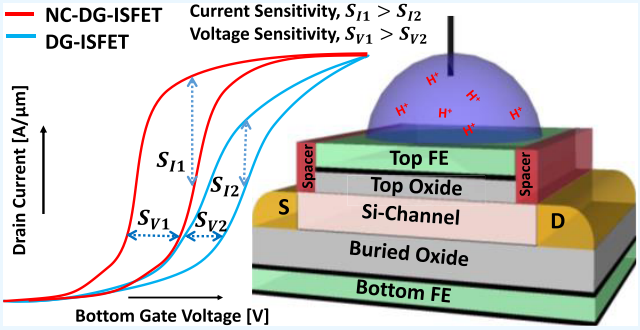

1. INTRODUCTION

Measurement of hydrogen ion concentration or pH plays a vital role in disease diagnostics, environmental monitoring, food processing, agriculture, pharmaceuticals, and other relevant industrial applications.[1,2] Electrochemical reactions involving pH changes were traditionally monitored via optical or electrochemical (potentiometric and voltammetric) measurement systems. However, despite offering high sensitivity, optical setups are bulky and require sophisticated and expensive instrumentation, while the three-electrode systems, in most cases, are not suitable for mass production and system integration.[3,4] In recent times, pH sensors based on ion-sensitive field-effect transistors (ISFETs) have attracted a great deal of interest due to their compact size, high sensitivity, fast response time, low cost, and compatibility with existing complementary metal-oxide semiconductor (CMOS) processes.[5,6] Moreover, ISFETs can be functionalized to detect a wide variety of biomolecules, making them useful for numerous biochemical applications. Unlike conventional metal-oxide semiconductor field-effect transistors (MOSFETs), the metal gate in ISFETs is replaced by a reference electrode, also known as the floating or fluid gate, dipped into an electrolyte solution. A fixed electrostatic potential is applied to the electrolytic solution by the reference electrode, which also enables the application of a fluid-gate bias (V_{FG}) to the ISFET. Changes in pH in the electrolyte solution modulate the surface potential (Ψ) at the interface of the electrolyte and the oxide, causing a shift in the threshold voltage and a corresponding change in drain current.[7]

The performance of ISFETs is characterized by their voltage and current sensitivities. In the constant current mode, the voltage sensitivity (S_V) of an ISFET is defined as the change in gate voltage (ΔV_G) that is needed to restore the drain current to its original value, following a change in pH (ΔpH), i.e., $S_V = (\Delta V_G)/(\Delta \text{pH})$. At room temperature, S_V for single-gated ISFETs is fundamentally limited to the Nernstian value of $[\ln(10)\ kT/q]$ per unit pH change or 59 mV/pH.[8] Over the past few decades, many research efforts have been directed toward enhancing the S_V of ISFETs beyond the Nernst limit. These include the use of new channel materials and sensing films, bias conditions, device geometries, and gate topologies of ISFETs.[9−12] One of the most widely used techniques to

Received: August 4, 2023
Revised: November 2, 2023
Accepted: November 9, 2023
Published: December 12, 2023

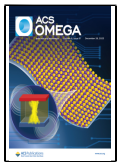

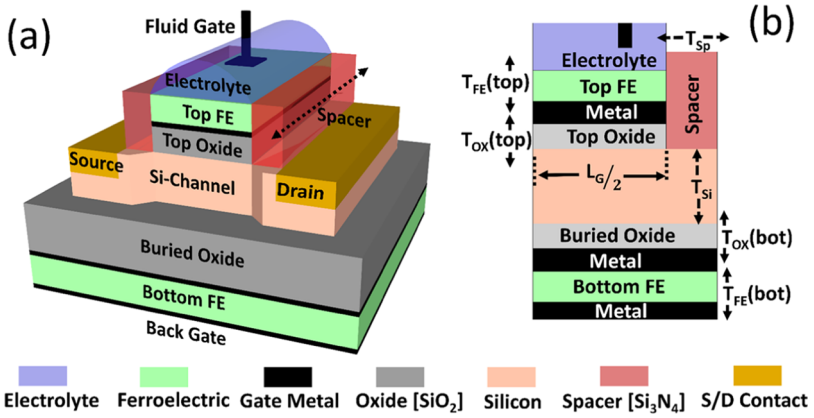

Figure 1. (a) Three-dimensional (3D) schematic (b) cross-sectional view of the proposed NC-DG-ISFET pH sensor showing the top and bottom gate stacks.

enhance S_V beyond the Nernst limit is to use a double-gated ISFET (DG-ISFET).[13−16] DG-ISFETs take advantage of the capacitive coupling between the top (fluid) and the bottom gates, allowing small changes in Ψ to be amplified without the need for additional amplifier circuits or extended gates.[17]

The current sensitivity (S_I) of an ISFET, at a fixed gate voltage, is defined as the relative change in drain current ($\Delta I_D/I_D$) caused by a change in pH (ΔpH). In practice, the maximum S_I in FET-based biosensors is limited by the transistor's subthreshold swing (SS), which at room temperature has a minimum value of 60 mV/dec. Enhancing S_I requires ISFETs with steep-slope transfer characteristics. Previous studies have demonstrated highly sensitive biosensors and pH sensors by exploiting the steep-switching characteristics of tunnel FETs.[18−20] More recently, researchers have focused on leveraging the steep-subthreshold swing in negative capacitance FETs (NCFETs) to boost the S_I of ISFETs in the weak inversion region.[21] The ultralow power application of NCFETs, attributed to the reduced SS, has been demonstrated in practical inverter ring oscillator circuits.[22] Following the same principle, the proposed NC-ISFETs can offer excellent noise performance and a higher overdrive of the sensor, also leading to low power consumption.[23] In our previous study, we used technology computer-aided design (TCAD) simulations to demonstrate a negative capacitance gate-all-around tunnel FET (NC-GAA-TFET)-based biosensor.[24] The proposed device combined the benefits of the NC effect and quantum mechanical band-to-band-tunneling to achieve S_I as high as 10^5, with excellent noise performance. However, despite the improvements in S_I, enhancing S_V beyond the Nernst limit, in NC-ISFETs, remained a challenge.

In this work, we propose a negative capacitance dual-gated ISFET (NC-DG-ISFET) where a thin layer of ferroelectric (FE) material is inserted into the top (fluid) and bottom gate stacks. The capacitive coupling between the two gates enhances the voltage sensitivity, while the current sensitivity increases due to the NC effect introduced by the FE layers. To the best of our knowledge, this work is the first use of the NC effect to simultaneously achieve high voltage and current sensitivities in DG-ISFET devices. The remainder of the review is organized as follows. Section 2 discusses the proposed device structure followed by the simulation approach and the calibration of the TCAD model. Section 3 presents an evaluation of the sensing performance of NC-DG-ISFET under different biasing modes. Finally, the key findings are summarized in Section 4.

2. DEVICE STRUCTURE AND SIMULATION APPROACH

Figure 1(a) shows the three-dimensional (3D) schematic of the simulated NC-DG-ISFET with its cross-section presented in Figure 1(b). Despite the promise of improved sensing performance, the experimental studies on NC-DG-ISFETs are yet to be conducted, due to the difficult fabrication process of a double gate structure,[25] as well as finding suitable gate dielectric and FE materials with excellent CMOS compatibility and immunity against chemical solutions. Moreover, thick body DG FETs can degrade device performance by making the coupling ratio unstable and producing leakage currents.[17] To overcome some of these challenges, the proposed NC-DG-ISFET can be fabricated on a silicon-on-insulator (SOI) substrate, following the process reported by Jang et al.[26] and Park et al.[27] with additional steps to incorporate the FE layer in both the top and the bottom gate stacks. Al-doped hafnium oxide (Al:HfO_2) is used as the FE material due to its considerable ferroelectric nature and high compatibility to existing CMOS processes.[28] The thin film of Al:HfO_2 can be grown using standard deposition techniques like atomic layer deposition (ALD) as described in detail by Nourbakhsh et al.[29] The top gate FE layer (Al:HfO_2) is in contact with the electrolyte solution, where a change in pH is modeled as a change in the surface potential at the FE/electrolyte interface. This is in line with previous studies that have reported highly sensitive ISFET[30] and NC-ISFET[21] with HfO_2 and Si:HfO_2 as the sensing membrane, respectively. The nominal device parameters used in the simulations are listed in Table 1.

In accordance with the previous reports[21,24] on NCFET-based biosensors, a ferroelectric-metal−insulator−semiconductor (FMIS) structure has been considered in this study. When a metal layer is introduced between the FE and the dielectric, gate leakage through the FE degrades the stability and reliability of the device by causing the polarization of the FE material to slip outside the stable negative slope region in the polarization vs electric field plot of the FE material.[31] Although gate leakage current can practically make the FMIS NCFETs unstable,[32] by discharging the polarization charges of the FE layer, the effect can be ignored for thicker gate oxides.[33,34] Moreover, Khan et al.[35] showed that stability concern due to gate leakage in FMIS structure can be resolved by appropriate

https://doi.org/10.1021/acsomega.3c05716
ACS Omega 2023, 8, 48756−48763

Table 1. Input Device Parameters Used in the TCAD Simulation

symbol	parameter	value
L_G	channel length	300 nm
T_{si}	channel thickness	20 nm
N_{ch}	channel doping	10^{16} cm^{-3}
$N_{S/D}$	source/drain doping	10^{20} cm^{-3}
T_{ox} (top)	top oxide thickness	10 nm
T_{ox} (bot)	bottom oxide thickness	100 nm
T_{FE} (top)	top FE thickness	60 nm
T_{FE} (bot)	bottom FE thickness	80 nm
T_{stern}	stern layer thickness	0.3 nm
L_{spacer}	spacer thickness	20 nm

work function engineering of metals used in the external electrode and the intermediate layer. Employing pulsed measurements to substantiate NC effects in FMIS configurations has also been reported, as fast pulsed biasing allows investigation of the device response before leakage can discharge the capacitors.[36,37] In addition, the internal metal layer between the FE and the gate oxide ensures uniform polarization in the FE material despite changes in drain bias and simplifies TCAD simulations by allowing the FE layer to be treated as a capacitor added in series with the underlying FET.[38]

The simulation of transport and electrostatic characteristics of the baseline ISFET was carried out with the help of ATLAS (SILVACO) TCAD. Previous studies have reported commercial TCAD-based models with accurate characterization of ISFETs.[39−41] In this method, the electrolyte is modeled by exploiting the similarity between the equations for mobile ions in the electrolyte and those for charge carriers in semiconductors. Thus, an intrinsic semiconductor with zero bandgap and a constant permittivity of water ($\varepsilon \approx 80$, water) is used to represent a monovalent symmetric (1:1) electrolyte within the TCAD framework. The relation between the effective density of states in the conduction (N_C in cm^{-3}) and valence bands (N_V in cm^{-3}) of the semiconductor and the molar ion concentration (c_o in mol/L) of the bulk electrolyte is given by

$$N_C = N_V = \begin{cases} 10^{-3}\cdot N_{Av}(c_o + cH_{bulk}), \text{ for } pH_{bulk} \le 7 \\ 10^{-3}\cdot N_{Av}\left(c_o + \dfrac{10^{-14}}{cH_{bulk}}\right), \text{ for } pH_{bulk} > 7 \end{cases} \quad (1)$$

where c_o is fixed at 10^{-3} mol/L, N_{Av} is the Avogadro's number, and $cH_{bulk} = [H^+_{bulk}] = 10^{-pHbulk}$ is the hydrogen ion concentration in the bulk electrolyte, normalized to 1 mol/L. The formulation of surface charge density at the FE/electrolyte interface is obtained from the well-known site-binding model.[42] This is implemented in TCAD with the help of user-defined interface acceptor and donor traps, with trap parameters being tuned with site-binding parameters of HfO_2.[43] The Stern layer, where the net ionic charge is zero, is represented by a thin semiconductor film with low density of states ($N_C = N_V$).[44] The Shockley−Read−Hall (SRH) and Auger recombination model,[45] Lombardi and field-dependent mobility model,[46] and dopant-dependent bandgap narrowing model[47] were considered in the simulation. Additionally, the Bohm quantum correction model was applied to account for quantum confinement at nanoscale dimensions.[48]

Current (I_D) and gate charge (Q_G) as a function of the applied gate bias are obtained from the self-consistent solution of Poisson's equations and current continuity equations. Extracted results are used to model the FE capacitor with the help of the single-domain phenomenological Landau-Khalatnikov (L-K) equation. The polarization (P) across the FE material is related to the external electric field (E_{ext}) by the equation[49]

$$E_{ext} = 2\alpha P + 4\beta P^3 + 6\gamma P^5 \quad (2)$$

where $\alpha = -3 \times 10^9$ m/F, $\beta = 6 \times 10^{11}$ m^5/C^{2}F, and $\gamma = 0$ are the Landau coefficients, representing bulk material parameters of Al:HfO_2. The voltage across the FE, V_{FE}, can be obtained from (eq 2) as

$$V_{FE} = [2\alpha Q_G + 4\beta Q_G^3]T_{FE} \quad (3)$$

with T_{FE} being the thickness of the FE layer. The effect of the depolarization field and gate leakage has been ignored to exclusively focus on sensing performance.

To validate the TCAD models that are used to simulate the proposed NC-DG-ISFET, we calibrate both the ISFET and NCFET models against experimental results reported in the literature. Figure 2(a) shows the calibration of the ISFET model[44] at different pH values, while calibration of the transfer characteristics of a planar NCFET device[50] is presented in Figure 2(b).

3. RESULTS AND DISCUSSION

The proposed NC-DG-ISFET is operated by sweeping the bottom gate voltage (V_{BG}) while holding the fluid gate at a fixed bias (V_{FG}). For a range of pH values, Figure 3(a) shows the transfer characteristics ($I_D - V_{BG}$) plot of a baseline DG-ISFET (i.e., a NC-DG-ISFET with T_{FE} (top) = T_{FE} (bot) = 0 nm) when V_{FG} = 1.0 V. A change in the pH of the electrolyte

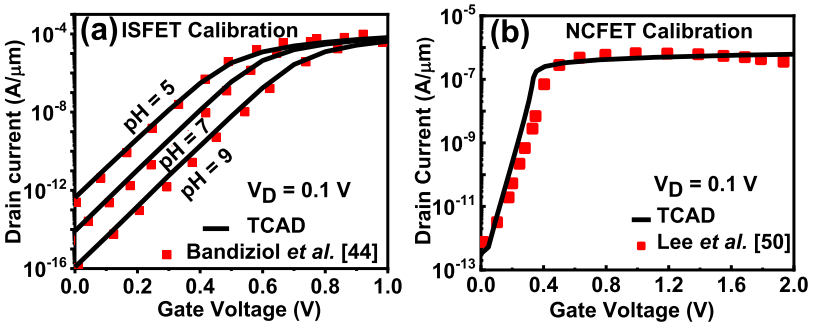

Figure 2. Calibration of the TCAD simulation results with experimental data for (a) ISFET and (b) NCFET.

https://doi.org/10.1021/acsomega.3c05716
ACS Omega 2023, 8, 48756−48763

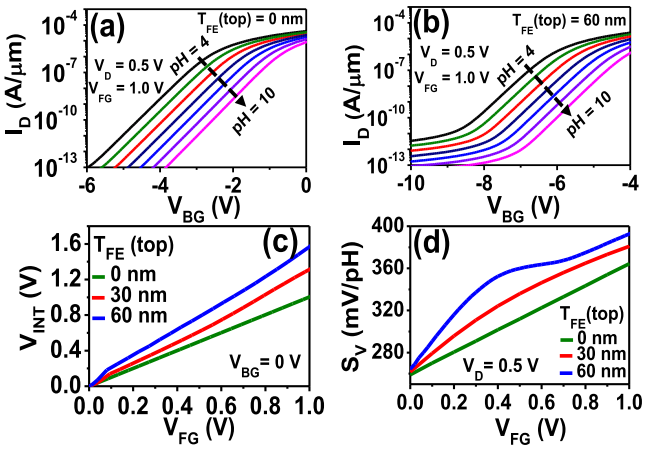

Figure 3. Transfer characteristics ($I_D - V_{BG}$) of DG-ISFET extracted at different pH values with top gate ferroelectric thickness, T_{FE} (top), taken as (a) 0 nm and (b) 60 nm at V_D = 0.5 V and V_{FG} = 1.0 V. (c) Potential drop (V_{INT}) across the internal metal gate as a function of fluid-gate voltage (V_{FG}) with back-gate bias (V_{BG}) set to 0 V and (d) voltage sensitivity (S_V) as a function of V_{FG} at V_D = 0.5 V for different values of T_{FE} (top). Bottom gate ferroelectric thickness, T_{FE} (bot), in (a–d) is kept at 0 nm.

solution modulates the surface charge at the interface of the FE and the electrolyte, causing a shift in the $I_D - V_{BG}$ characteristics. For the same pH range, Figure 3(b) illustrates the $I_D - V_{BG}$ behavior at V_{FG} = 1.0 V, with T_{FE} (top) = 60 nm and T_{FE} (bot) = 0 nm, clearly showing the left shift of the transfer characteristics when compared to the baseline device in Figure 3(a). This shift can be explained in terms of the NC effect brought about by inclusion of the FE layer in the top gate stack.

The use of negative FE capacitance ($C_{FE} < 0$) lowers the subthreshold swing (SS) of the NC-DG-ISFET device by making the total capacitance, $C_{total} = (C_{FE}^{-1} + C_{ISFET}^{-1})^{-1}$, larger than the capacitance of the baseline counterpart (C_{ISFET}). Here, C_{ISFET} consists of the electrolyte and the MOS capacitance connected in series and is given by $C_{ISFET} = (C_{electrolyte}^{-1} + C_{MOS}^{-1})^{-1}$. SS can be lowered by matching C_{FE} with C_{MOS}, which can be done by varying the T_{FE} since C_{FE} varies inversely with T_{FE}. Although a thicker FE enhances the NC effect, increasing T_{FE} over a critical thickness introduces hysteresis and makes the device unstable. Therefore, capacitance matching was carefully performed by extracting the C_{MOS} at low drain bias (i.e., the linear region of the transfer characteristics) and T_{FE} was chosen appropriately to avoid hysteresis at all biases. As V_{FG} increases (with V_{BG} = 0 V), the presence of the FE increases the potential drop (V_{int}) across the internal metal gate, as shown in Figure 3(c). The thicker the FE layer, the higher the V_{INT} at any given V_{FG}. The voltage sensitivity, S_V, can be expressed as[8]

$$S_V = \frac{\Delta V_{BG}}{\Delta pH} = \frac{\Delta V_{FG}}{\Delta pH} \times \left(\frac{C_{top}}{C_{bot}}\right) \quad (4)$$

where $\Delta V_{BG}/\Delta pH$ and $\Delta V_{FG}/\Delta pH$ represent the changes in bottom and fluid-gate bias with changes in pH, and C_{bot} and C_{top} denote the capacitive coupling of the Si channel with the bottom and top gates, respectively. At low V_{FG}, the top channel is under depletion and the bottom channel is under inversion such that the Si body capacitance contributes to C_{top}, lowering the value of C_{top} and S_V. Higher V_{FG} (thicker T_{FE} (top)) drives the top channel to inversion, eliminating the effect of the Si body capacitance and increasing the S_V, as shown in Figure 3(d) for different values of T_{FE}. The highest value of T_{FE} (top) is fixed at 60 nm because beyond this value the device shows hysteresis and becomes unstable. It is obvious from Figure 3(d) that the inclusion of the FE layer in the top gate stack significantly boosts the S_V of a baseline DG-ISFET at a higher fluid-gate bias.

Next, we investigate the effect of adding FE layers in both the bottom and top gate stacks. Figure 4(a) shows the transfer characteristics ($I_D - V_{BG}$ at V_{FG} = 1.0 V) of the NC-DG-ISFET with T_{FE} (top) = 60 nm and T_{FE} (bot) = 80 nm. With T_{FE} (top) fixed at 60 nm, the thickness of the bottom FE, T_{FE} (bot), is varied to obtain the lowest SS, without causing any hysteresis. Figure 4(b) illustrates how the SS changes with T_{FE} (bot) when T_{FE} (top) = 60 nm. Results show that, in comparison to T_{FE} (bot) = 0 nm, the *SS* of the NC-DG-ISFET device is reduced by approximately 30 and 51% when T_{FE} (bot) = 40 and 80 nm, respectively.

The reduction in SS, due to the NC effect, leads to enhanced current sensitivity (S_I) in the subthreshold regime, which is consistent with our recent study on NC-based gate-all-around tunnel FET biosensors.[24] Figure 5(a,b) summarizes the current sensitivities obtained from the subthreshold and the saturation region of the transfer characteristics, respectively. Compared to the baseline device, which has T_{FE} (top) = T_{FE} (bot) = 0 nm, there is a 3× and 5× enhancement in S_I in the subthreshold region, when T_{FE} (bot) = 40 and 80 nm, respectively. In both cases, T_{FE} (top) was fixed at 60 nm.

For any given pH value, the back-gate voltage (V_{BG}), at a fixed drain current (in this case, 10^{-9} A), is defined as the

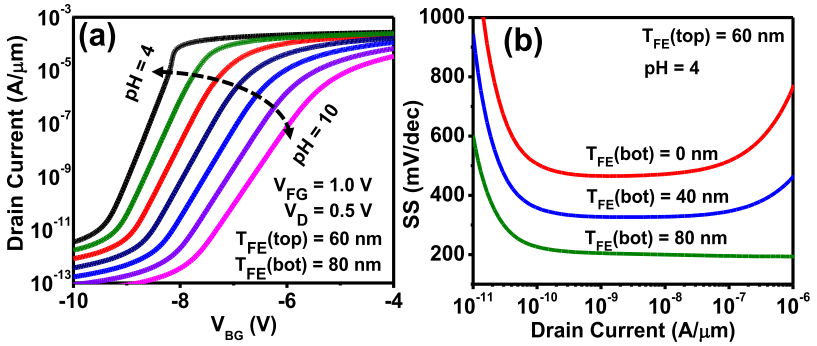

Figure 4. (a) Transfer characteristics ($I_D - V_{BG}$) of NC-DG-ISFET for different pH values with T_{FE} (bot) = 80 nm and T_{FE} (top) = 60 nm; (b) SS vs I_D of NC-DG-ISFET for varying T_{FE} (bot), at pH = 4, with T_{FE} (top) fixed at 60 nm.

https://doi.org/10.1021/acsomega.3c05716
ACS Omega 2023, 8, 48756−48763

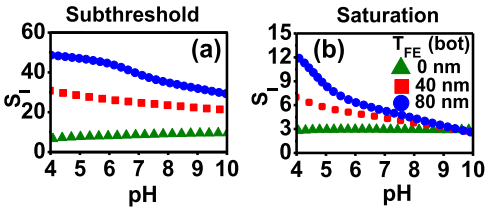

Figure 5. Current sensitivity (S_I) of NC-DG-ISFET measured in (a) subthreshold and (b) saturation region of operation, as a function of pH at T_{FE} (bot) = 0, 40, and 80 nm. In each case, T_{FE} (top) = 60 nm.

responsive voltage (V_R).[12] Figure 6(a,b) shows ΔV_R vs ΔpH plots in the subthreshold and saturation regions, respectively.

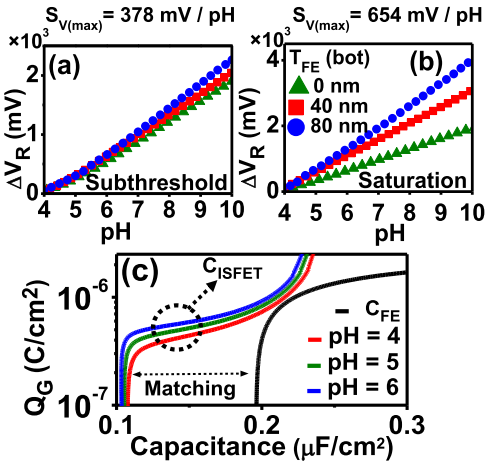

Figure 6. (a) Voltage sensitivity (S_V) measured in the (a) subthreshold and (b) saturation region; (c) capacitance matching between C_{ISFET} and C_{FE} for different pH values at V_D = 0.05 V.

S_V, which is obtained from the slope, increases with increasing T_{FE} (bot), especially in the saturation region. Any change in V_R (i.e., ΔV_R), due to a change in pH (i.e., ΔpH), is proportional to the shift in internal voltage (i.e., ΔΨ) where $\Delta\Psi = 2.303(k_BT/q)\Delta pH$. ΔΨ is identical for the baseline and NC device. However, the dynamic balance between the capacitive coupling of the two gates of DG-ISFET and the capacitance matching between C_{FE} and C_{ISFET} governs the voltage sensitivity of the NC-DG-ISFET pH sensor. Figure 6(c) shows the capacitance matching between C_{FE} and C_{ISFET} for different pH values. C_{ISFET} varies with changes in pH, which, in turn, determines the internal voltage amplification and therefore affects the shifts between curves for different pH values in the NC-DG-ISFET. Hence, changes in pH induce variation in both the surface charge density at the oxide-electrolyte interface and in the potential in the internal node, leading to a 2× increase in S_V (with respect to the baseline device) in the saturation region when T_{FE} (bot) = 80 nm and T_{FE} (top) = 60 nm.

For realistic performance benchmarking, S_V is taken as the figure-of-merit and maximum S_V of the proposed NC-DG-ISFET device is compared with the voltage sensitivities obtained from fabricated baseline dual-gated ISFETs[9,10,16,26,51−55] and a fabricated NC-ISFET[21] reported in the literature. Some of these results are summarized in the bar plot in Figure 7. Until now, only Bellando et al.[21] experimentally demonstrated a practical NC-ISFET device and reported a S_V of 14 mV/pH, which is also included in the

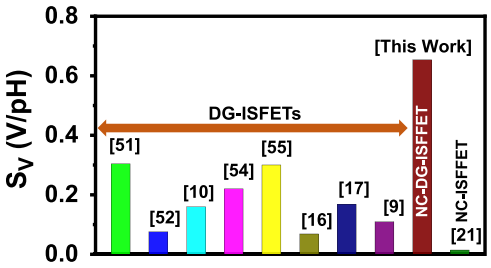

Figure 7. Voltage sensitivity (S_V) of the proposed NC-DG-ISFET with respect to other DG-ISFETs and a NC-ISFET reported in the literature.

bar plot to provide a clearer perspective on the superiority of the proposed design. From Figure 7, it is obvious that the NC-DG-ISFET in this study shows significantly higher S_V values compared to some of the existing dual-gated ISFETs and NC-ISFET pH sensors.

Figures 8 and 9 illustrate the influence of critical device parameters such as channel thickness (T_{si}) and channel length

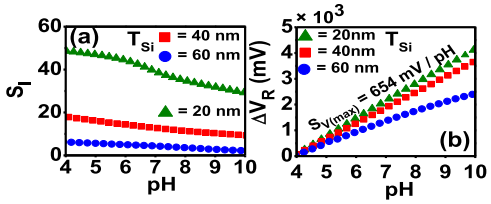

Figure 8. Variation of (a) S_I and (b) S_V of the proposed NC-DG-ISFET as a function of pH for varying silicon channel thickness (T_{si}).

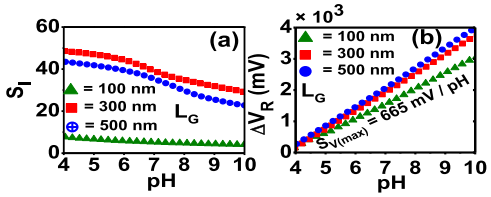

Figure 9. Variation of (a) S_I and (b) ΔV_R as a function of pH for varying channel length (L_G).

(L_G) on the current and voltage sensitivities of the NC-DG-ISFET sensor. This is obtained by examining how the transfer characteristics in the subthreshold region of operation change with varying T_{si} and L_G. For instance, a lower value of T_{si} improves the control of the gates and reduces SS, which accounts for enhanced S_I in devices with thinner channels. As illustrated in Figure 8(a), approximately 8× increase in S_I is achieved when T_{si} is reduced from 60 to 20 nm. Moreover, decreasing T_{si} results in partial to full depletion of the channel, which ensures better capacitive coupling, leading to increased S_V of the device, as shown in Figure 8(b).

Decreasing L_G, on the other hand, results in an increase in leakage current and degradation of SS, which leads to a 6× increase in S_I, when L_G increases from 100 to 300 nm, as shown in Figure 9(a). Figure 9(b) shows the shift in responsive voltage (ΔV_R) due to the pH change, calculated with respect to pH = 4. The slope of the graph in Figure 9(b), which gives S_V, increases with decreasing L_G, reaching its maximum value of 665 mV/pH at L_G = 100 nm.

It is well established that the variation of operating temperature significantly influences the performance of

https://doi.org/10.1021/acsomega.3c05716
ACS Omega 2023, 8, 48756−48763

ISFETs.[56] A recent study has demonstrated changes in output and transfer characteristics of ISFETs, with changes in temperature such that the drain current decreases when temperature is increased.[57] This is due to the change in the mobility and the corresponding shift in threshold voltage at high temperatures. Consequently, both the voltage and current sensitivities increase with an increase in temperature in baseline DG-ISFETs. The inclusion of NC effect, however, results in an opposite trend where S_V decreases with increase in temperature. This is because, compared to baseline devices, the *SS* in NCFETs increases more rapidly with the increase in temperature leading to a faster degradation of device performance.[58]

4. CONCLUSIONS

In summary, we have used TCAD simulations to demonstrate a novel dual-gated pH-sensing NC-DG-ISFET that can achieve enhanced current and voltage sensitivities by simply incorporating an FE layer in the gate stacks of conventional DG-ISFETs. Compared to baseline DG-ISFETs, a maximum of 5× improvement in S_I was achieved when the thicknesses of the FE layer in the top and bottom gates were 60 and 80 nm, respectively. Under the same conditions, S_V is enhanced by a factor of 2, with respect to the baseline device. Although a thicker FE may introduce a stronger NC effect, a further increase in FE thickness causes hysteresis and makes the device unstable. When benchmarked against other ISFETs, reported in the literature, the proposed NC-DG-ISFET shows superior performance in terms of S_V. However, an increase in operating temperature can degrade SS and lower the S_V of NC-DG-ISFETs. Device parameters, like T_{si} and L_G, can be optimized to further tune the S_I and S_V for maximum sensitivity. We believe that the results presented in this work will aid in the development of the next generation of highly sensitive ISFETs that exploit the sub-60 mV/decade switching behavior of NCFETs.

AUTHOR INFORMATION

Corresponding Author

Mainul Hossain − *Department of Electrical and Electronic Engineering, University of Dhaka, Dhaka 1000, Bangladesh;* orcid.org/0000-0001-9011-9029; Email: mainul.eee@du.ac.bd

Authors

Fahimul Islam Sakib − *Department of Electrical and Electronic Engineering, University of Dhaka, Dhaka 1000, Bangladesh;* orcid.org/0000-0003-3257-1396

Md. Azizul Hasan − *Department of Electrical and Electronic Engineering, University of Dhaka, Dhaka 1000, Bangladesh; Department of Electrical and Computer Engineering, North Carolina State University, Raleigh, North Carolina 27606, United States;* orcid.org/0000-0003-1721-5916

Mumtahena Diyan Mohona − *Department of Electrical and Electronic Engineering, University of Dhaka, Dhaka 1000, Bangladesh;* orcid.org/0009-0007-5977-1984

Complete contact information is available at: https://pubs.acs.org/10.1021/acsomega.3c05716

Author Contributions

§F.I.S. and M.A.H. contributed equally to this work.

Notes

The authors declare no competing financial interest.

ACKNOWLEDGMENTS

The authors thankfully acknowledge the financial support from the University Grants Commission (UGC) of Bangladesh Research Fund 2022−2023 for the University of Dhaka. In addition, the authors are also grateful to Fab Lab DU, at University of Dhaka and Bangladesh Research and Education Network (BdREN) for providing the necessary computational resources for this simulation study.

REFERENCES

(1) Cao, S.; Sun, P.; Xiao, G.; Tang, Q.; Sun, X.; Zhao, H.; Zhao, S.; Lu, H.; Yue, Z. ISFET-based Sensors for (Bio)Chemical Applications: A Review. *Electrochem. Sci. Adv.* **2023**, No. e2100207.

(2) Khan, M. I.; Mukherjee, K.; Shoukat, R.; Dong, H. A Review on pH Sensitive Materials for Sensors and Detection Methods. *Microsyst. Technol.* **2017**, *23*, 4391−4404.

(3) Steinegger, A.; Wolfbeis, O. S.; Borisov, S. M. Optical Sensing and Imaging of pH Values: Spectroscopies, Materials, and Applications. *Chem. Rev.* **2020**, *120*, 12357−12489.

(4) Vivaldi, F.; Salvo, P.; Poma, N.; Bonini, A.; Biagini, D.; Del Noce, L.; Melai, B.; Lisi, F.; Di Francesco, F. Recent Advances in Optical, Electrochemical and Field Effect pH Sensors. *Chemosensors* **2021**, *9* (2), No. 33.

(5) Sinha, S.; Pal, T. A Comprehensive Review of FET-based pH Sensors: Materials, Fabrication Technologies, and Modeling. *Electrochem. Sci. Adv.* **2022**, No. e2100147.

(6) Syu, Y.-C.; Hsu, W.-E.; Lin, C.-T. Review-Field-Effect Transistor Biosensing: Devices and Clinical Applications. *ECS J. Solid State Sci. Technol.* **2018**, *7*, Q3196−Q3207.

(7) Kaisti, M. Detection Principles of Biological and Chemical FET Sensors. *Biosens. Bioelectron.* **2017**, *98*, 437−448.

(8) Go, J.; Nair, P. R.; Alam, M. A. Theory of Signal and Noise in Double-Gated Nanoscale Electronic pH Sensors. *J. Appl. Phys.* **2012**, *112*, No. 034516.

(9) Kumar, N.; Kumar, J.; Panda, S. Enhanced pH Sensitivity over the Nernst Limit of Electrolyte Gated A-IGZO Thin Film Transistor Using Branched Polyethylenimine. *RSC Adv.* **2016**, *6*, 10810−10815.

(10) Kumar, N.; Kumar, J.; Panda, S. Back-Channel Electrolyte-Gated a-IGZO Dual-Gate Thin-Film Transistor for Enhancement of pH Sensitivity Over Nernst Limit. *IEEE Electron Device Lett.* **2016**, *37*, 500−503.

(11) Jung, S. H.; Seo, Y. M.; Gu, T.; Jang, W.; Kang, S. G.; Hyeon, Y.; Hyun, S. H.; Lee, J. H.; Whang, D. Super-Nernstian pH Sensor Based on Anomalous Charge Transfer Doping of Defect-Engineered Graphene. *Nano Lett.* **2021**, *21*, 34−42.

(12) Dwivedi, P.; Singh, R.; Chauhan, Y. S. Crossing the Nernst Limit (59 mV/pH) of Sensitivity through Tunneling Transistor-Based Biosensor. *IEEE Sens. J.* **2021**, *21*, 3233−3240.

(13) Duarte-Guevara, C.; Lai, F. L.; Cheng, C. W.; Reddy, B.; Salm, E.; Swaminathan, V.; Tsui, Y. K.; Tuan, H. C.; Kalnitsky, A.; Liu, Y. S.; Bashir, R. Enhanced Biosensing Resolution with Foundry Fabricated Individually Addressable Dual-Gated ISFETs. *Anal. Chem.* **2014**, *86*, 8359−8367.

(14) Tamersit, K.; Djeffal, F. Double-Gate Graphene Nanoribbon Field-Effect Transistor for DNA and Gas Sensing Applications: Simulation Study and Sensitivity Analysis. *IEEE Sens. J.* **2016**, *16*, 4180−4191.

(15) Go, J.; Nair, P. R.; Reddy, B.; Dorvel, B.; Bashir, R.; Alam, M. A.*Beating the Nernst Limit of 59 mV/pH with Double-Gated Nano-Scale Field-Effect Transistors and Its Applications to Ultra-Sensitive DNA Biosensors*, 2010 International Electron Devices Meeting; IEEE, 2010; pp 8.7.1−8.7.4.

(16) Ahn, J. H.; Kim, J. Y.; Seol, M. L.; Baek, D. J.; Guo, Z.; Kim, C. H.; Choi, S. J.; Choi, Y. K. A PH Sensor with a Double-Gate Silicon

https://doi.org/10.1021/acsomega.3c05716
ACS Omega 2023, 8, 48756−48763

Nanowire Field-Effect Transistor. *Appl. Phys. Lett.* **2013**, *102*, No. 083701.
(17) Jang, H. J.; Cho, W. J. Performance Enhancement of Capacitive-Coupling Dual-Gate Ion-Sensitive Field-Effect Transistor in Ultra-Thin-Body. *Sci. Rep.* **2014**, *4*, No. 5284.
(18) Sarkar, D.; Banerjee, K. Proposal for Tunnel-Field-Effect-Transistor as Ultra-Sensitive and Label-Free Biosensors. *Appl. Phys. Lett.* **2012**, *100*, No. 143108.
(19) Lee, R.; Kwon, D. W.; Kim, S.; Kim, D. H.; Park, B. G. Investigation of Feasibility of Tunneling Field Effect Transistor (TFET) as Highly Sensitive and Multi-Sensing Biosensors. *J. Semicond. Technol. Sci.* **2017**, *17*, 141−146.
(20) Kim, S.; Lee, R.; Kwon, D.; Kim, T. H.; Park, T. J.; Choi, S. J.; Mo, H. S.; Kim, D. H.; Park, B. G. Multiplexed Silicon Nanowire Tunnel FET-Based Biosensors with Optimized Multi-Sensing Currents. *IEEE Sens. J.* **2021**, *21*, 8839−8846.
(21) Bellando, F.; Dabhi, C. K.; Saeidi, A.; Gastaldi, C.; Chauhan, Y. S.; Ionescu, A. M. Subthermionic Negative Capacitance Ion Sensitive Field-Effect Transistor. *Appl. Phys. Lett.* **2020**, No. 173503.
(22) Krivokapic, Z.; Rana, U.; Galatage, R.; Razavieh, A.; Aziz, A.; Liu, J.; Shi, J.; Kim, H. J.; Sporer, R.; Serrao, C.*14nm Ferroelectric FinFET Technology with Steep Subthreshold Slope for Ultra Low Power Applications*, 2017 IEEE International Electron Devices Meeting (IEDM); IEEE, 2017; pp 15.1.1−15.1.4.
(23) Zagni, N.; Pavan, P.; Alam, M. A. Two-Dimensional MoS_2 Negative Capacitor Transistors for Enhanced (Super-Nernstian) Signal-to-Noise Performance of next-Generation Nano Biosensors. *Appl. Phys. Lett.* **2019**, *114*, No. 233102.
(24) Sakib, F. I.; Hasan, M. A.; Hossain, M. Negative Capacitance Gate-All-Around Tunnel FETs for Highly Sensitive Label-Free Biosensors. *IEEE Trans. Electron Devices* **2022**, *69*, 311−317.
(25) Chung, T. M.; Olbrechts, B.; Södervall, U.; Bengtsson, S.; Flandre, D.; Raskin, J. P. Planar Double-Gate SOI MOS Devices: Fabrication by Wafer Bonding over Pre-Patterned Cavities and Electrical Characterization. *Solid-State Electron.* **2007**, *51*, 231−238.
(26) Jang, H. J.; Cho, W. J. Fabrication of High-Performance Fully Depleted Silicon-on-Insulator Based Dual-Gate Ion-Sensitive Field-Effect Transistor beyond the Nernstian Limit. *Appl. Phys. Lett.* **2012**, *100*, No. 073701.
(27) Park, J. K.; Jang, H. J.; Park, J. T.; Cho, W. J. SOI Dual-Gate ISFET with Variable Oxide Capacitance and Channel Thickness. *Solid-State Electron.* **2014**, *97*, 2−7.
(28) Xia, Y.; Liu, L.; Tao, X.; Tian, Y.; Xu, J. P. Improved Performance of MoS_2 Negative-Capacitance Field-Effect Transistors by Optimizing Gate-Stack of Al-Doped HfO_2/$Al2O_3$. *IEEE Trans. Electron Devices* **2023**, *70*, 782−788.
(29) Nourbakhsh, A.; Zubair, A.; Joglekar, S.; Dresselhaus, M.; Palacios, T. Subthreshold Swing Improvement in MoS_2 Transistors by the Negative-Capacitance Effect in a Ferroelectric Al-Doped-HfO_2/HfO_2 Gate Dielectric Stack. *Nanoscale* **2017**, *9*, 6122−6127.
(30) Bhatt, D.; Panda, S. High Sensitivity of Dual Gate ISFETs Using $HfO_2$and HfO_2/Y_2O_3Gate Dielectrics. *ACS Appl. Electron. Mater.* **2021**, *3*, 2818−2824.
(31) Min, J.; Shin, C. MFMIS Negative Capacitance FinFET Design for Improving Drive Current. *Electronics* **2020**, *9*, No. 1423.
(32) Khan, A. I.; Radhakrishna, U.; Chatterjee, K.; Salahuddin, S.; Antoniadis, D. A. Negative Capacitance Behavior in a Leaky Ferroelectric. *IEEE Trans. Electron Devices* **2016**, *63*, 4416−4422.
(33) Si, M.; Su, C. J.; Jiang, C.; Conrad, N. J.; Zhou, H.; Maize, K. D.; Qiu, G.; Wu, C. T.; Shakouri, A.; Alam, M. A.; Ye, P. D. Steep-Slope Hysteresis-Free Negative Capacitance MoS_2 Transistors. *Nat. Nanotechnol.* **2018**, *13*, 24−28.
(34) Jiang, C.; Si, M.; Liang, R.; Xu, J.; Ye, P. D.; Alam, M. A. A Closed Form Analytical Model of Back-Gated 2-D Semiconductor Negative Capacitance Field Effect Transistors. *IEEE J. Electron Devices Soc.* **2018**, *6*, 189−194.
(35) Khan, A. I.; Radhakrishna, U.; Salahuddin, S.; Antoniadis, D. Work Function Engineering for Performance Improvement in Leaky Negative Capacitance FETs. *IEEE Electron Device Lett.* **2017**, *38*, 1335−1338.
(36) Ng, K.; Hillenius, S. J.; Gruverman, A. Transient Nature of Negative Capacitance in Ferroelectric Field-Effect Transistors. *Solid State Commun.* **2017**, *265*, 12−14.
(37) Hoffmann, M.; Fengler, F. P. G.; Herzig, M.; Mittmann, T.; Max, B.; Schroeder, U.; Negrea, R.; Pintilie, L.; Slesazeck, S.; Mikolajick, T. Unveiling the Double-Well Energy Landscape in a Ferroelectric Layer. *Nature* **2019**, *565*, 464−467.
(38) Pahwa, G.; Agarwal, A.; Chauhan, Y. S. Numerical Investigation of Short-Channel Effects in Negative Capacitance MFIS and MFMIS Transistors: Subthreshold Behavior. *IEEE Trans. Electron Devices* **2018**, *65*, 5130−5136.
(39) Mohammadi, E.; Manavizadeh, N. An Accurate TCAD-Based Model for ISFET Simulation. *IEEE Trans. Electron Devices* **2018**, *65*, 3950−3956.
(40) Pittino, F.; Palestri, P.; Scarbolo, P.; Esseni, D.; Selmi, L. Models for the Use of Commercial TCAD in the Analysis of Silicon-Based Integrated Biosensors. *Solid-State Electron.* **2014**, *98*, 63−69.
(41) Choi, B.; Lee, J.; Yoon, J.; Ahn, J.-H.; Park, T. J.; Kim, D. M.; Kim, D. H.; Choi, S.-J. TCAD-Based Simulation Method for the Electrolyte−Insulator−Semiconductor Field-Effect Transistor. *IEEE Trans. Electron Devices* **2015**, *62*, 1072−1075.
(42) Yates, D. E.; Levine, S.; Healy, T. W. Site-Binding Model of the Electrical Double Layer at the Oxide/Water Interface. *J. Chem. Soc., Faraday Trans. 1* **1974**, *70*, 1807−1818.
(43) Narang, R.; Saxena, M.; Gupta, M. Analytical Model of pH Sensing Characteristics of Junctionless Silicon on Insulator ISFET. *IEEE Trans. Electron Devices* **2017**, *64*, 1742−1750.
(44) Bandiziol, A.; Palestri, P.; Pittino, F.; Esseni, D.; Selmi, L. A TCAD-Based Methodology to Model the Site-Binding Charge at ISFET/Electrolyte Interfaces. *IEEE Trans. Electron Devices* **2015**, *62*, 3379−3386.
(45) Liu, C.; Chen, P.-G.; Xie, M.-J.; Liu, S.-N.; Lee, J.-W.; Huang, S.-J.; Liu, S.; Chen, Y.-S.; Lee, H.-Y.; Liao, M.-H.; Chen, P.-S.; Lee, M.-H. Simulation-Based Study of Negative-Capacitance Double-Gate Tunnel Field-Effect Transistor with Ferroelectric Gate Stack. *Jpn. J. Appl. Phys.* **2016**, *55*, No. 04EB08.
(46) Darwish, M. N.; Lentz, J. L.; Pinto, M. R.; Zeitzoff, P. M.; Krutsick, T. J.; Vuong, H. H. An Improved Electron and Hole Mobility Model for General Purpose Device Simulation. *IEEE Trans. Electron Devices* **1997**, *44*, 1529−1538.
(47) Stefanakis, D.; Zekentes, K. TCAD Models of the Temperature and Doping Dependence of the Bandgap and Low Field Carrier Mobility in 4H-SiC. *Microelectron. Eng.* **2014**, *116*, 65−71.
(48) Hamid, F. K. A.; Johari, Z.; Alias, N. E.; Lim, W. H.; Sultan, S. M.; Leong, W. S.; Ismail, R. Modeling of Inversion and Centroid Charges of Long Channel Strained-Silicon Surrounding Gate MOSFETs Incorporating Quantum Effects. *Semicond. Sci. Technol.* **2020**, *35*, No. 025010.
(49) Gaidhane, A. D.; Pahwa, G.; Verma, A.; Chauhan, Y. S. Compact Modeling of Drain Current, Charges, and Capacitances in Long-Channel Gate-All-Around Negative Capacitance MFIS Transistor. *IEEE Trans. Electron Devices* **2018**, *65*, 2024−2032.
(50) Lee, M. H.; Chen, P.; Liu, C.; Chu, K.; Cheng, C.; Xie, M.; Liu, S.; Lee, J.; Huang, S.; Liao, M.; Tang, M.; Li, K.; Chen, M.*Prospects for Ferroelectric HfZrOx FETs with Experimentally CET = 0.98nm, SSfor=42mV/Dec, SSrev=28mV/Dec, Switch-off < 0.2V, and Hysteresis-Free Strategies*, 2015 IEEE International Electron Devices Meeting (IEDM); IEEE, 2015; pp 22.5.1−22.5.4.
(51) Jeon, J. H.; Park, J. T.; Cho, W. J. *Coplanar Dual Gates Silicon-on-Insulator Based Ultra-Sensitive Ion-Sensitive Field-Effect Transistors for Point-of-Care Biosensor Platform*, 2019 Joint International EUROSOI Workshop and International Conference on Ultimate Integration on Silicon (EUROSOI-ULIS); IEEE, 2019; pp 1−4.
(52) Pavlidis, S.; Getz, P.; Hagen, J.; Kelley-Loughnane, N.; Bayraktaroglu, B.; Brand, O. *Investigating Thin Film Passivations for IGZO Dual Gate pH Sensors Fabricated at Low Temperature*, 2015 Transducers - 2015 18th International Conference on Solid-State

https://doi.org/10.1021/acsomega.3c05716
ACS Omega 2023, 8, 48756−48763

Sensors, Actuators and Microsystems (TRANSDUCERS); IEEE, 2015; pp 1334−1337.
(53) Knopfmacher, O.; Tarasov, A.; Fu, W.; Wipf, M.; Niesen, B.; Calame, M.; Schönenberger, C. Nernst Limit in Dual-Gated Si-Nanowire FET Sensors. *Nano Lett.* **2010**, *10*, 2268−2274.
(54) Reddy, B.; Dorvel, B. R.; Go, J.; Nair, P. R.; Elibol, O. H.; Credo, G. M.; Daniels, J. S.; Chow, E. K. C.; Su, X.; Varma, M.; Alam, M. A.; Bashir, R. High-k Dielectric Al2O3 Nanowire and Nanoplate Field Effect Sensors for Improved pH Sensing. *Biomed. Microdevices* **2011**, *13*, 335−344.
(55) Liu, N.; Hui Liu, Y.; Feng, P.; Qiang Zhu, L.; Shi, Y.; Wan, Q. Enhancing the pH Sensitivity by Laterally Synergic Modulation in Dual-Gate Electric-Double-Layer Transistors. *Appl. Phys. Lett.* **2015**, *106*, No. 073507.
(56) Chou, J. C.; Wang, Y. F.; Lin, J. S. Temperature Effect of A-Si:H pH-ISFET. *Sens. Actuators, B* **2000**, *62*, 92−96.
(57) Datar, R.; Bacher, G. Influence of Gate Material, Geometry, and Temperature on ISFET Performance in pH Sensing Applications. *Silicon* **2023**, *15*, 5393−5405.
(58) Wang, C.; Wu, J.; Yu, H.; Han, G.; Miao, X.; Wang, X. Effects of Temperature on the Performance of $Hf_{0.5}Zr_{0.5}O_2$-Based Negative Capacitance FETs. *IEEE Electron Device Lett.* **2020**, *41*, 1625−1628.

https://doi.org/10.1021/acsomega.3c05716
ACS Omega 2023, 8, 48756−48763